Published by :
https://www.ijert.org/
An International Peer-Reviewed Journal

International Journal of Engineering Research & Technology (IJERT)
ISSN: 2278-0181
Vol. 15 Issue 10 , October - 2026

Manganese Dioxide - Based Photocatalytic Oxidation Processes for the Removal of Ciprofloxacin from Water: Materials, Mechanisms and Perspectives

Padmaja Vempalli
Research Scholar, JNTU, Ananthapuram
Andhra Pradesh, India

Dr. P. Sri Chandana
Professor, AITS, Kadapa
Andhra Pradesh, India

Abstract: Ciprofloxacin (CIP), a broad-spectrum fluoroquinolone, is one of the most commonly detected antibiotics in surface waters and wastewater, contributing to ecological risks and the selection of antibiotic-resistant bacteria and genes. Various methods, including adsorption, photocatalysis, persulfate-based oxidation, and electrochemical oxidation, have been employed for its removal. Manganese dioxide (MnO_2) is an earth-abundant, low-toxicity, polymorphic oxide characterized by a narrow band gap (typically 1–2 eV), a rich Mn(IV)/Mn(III)/Mn(II) redox chemistry, and strong surface reactivity towards phenolic, anilinic, and amine-containing micropollutants. This review synthesizes evidence on (i) the occurrence, risk, and resistance associated with CIP, (ii) adsorptive and photocatalytic benchmarks for CIP, (iii) the structure–property relationships of α-, β-, γ-, δ-, and ε-MnO_2, (iv) the dark and light-driven transformation of pharmaceuticals on MnO_2, and (v) Mn-based catalysts that directly degrade CIP, including Mn/Co oxide photocatalysts and MnO_2-activated peroxymonosulfate (PMS) systems. In the literature, δ-MnO_2 and ε-MnO_2 are identified as the most reactive polymorphs. The oxidation process, including piperazine-ring cleavage, hydroxylation, and F/OH substitution in CIP transformation, is driven by reactive oxygen species (h+, OH, $O_2^{\cdot-}$, $^1O_2$) and Mn(III) intermediates. However, there is a significant gap in research regarding direct, light-driven CIP degradation by pristine MnO_2 polymorphs. We propose research priorities focusing on the mechanism, toxicity, real-water testing, and scale-up.

Keywords: ciprofloxacin, manganese dioxide, photocatalysis, peroxymonosulfate, reactive oxygen species, fluoroquinolone, water treatment

1. INTRODUCTION

Antibiotics are extensively utilized in both human and veterinary medicine. Due to incomplete metabolism, they enter wastewater and receiving waters in their original or transformed forms. Monitoring of Hong Kong's Kai Tak River nullah, which receives treated effluent from two wastewater treatment plants, revealed median concentrations of approximately 1694 ng L^{-1} for CIP and 632 ng L^{-1} for clarithromycin. CIP and clarithromycin are identified as the primary contributors to ecological risk for aquatic organisms [1]. Even at these concentrations, residues maintain antibiotic-resistance genes (ARGs) and resistant bacteria [1]. In clinical settings, ciprofloxacin (CIP) has lost efficacy due to extensive resistance, prompting the use of machine-learning tools to predict resistant infections [2]. Thus, controlling CIP at its environmental source is integral to a comprehensive antimicrobial-resistance strategy. Conventional biological treatments do not completely remove fluoroquinolones, necessitating advanced technologies. Reviews on antibiotic abatement highlight semiconductor photocatalysis for its ability to utilize sunlight, operate under ambient conditions, and mineralize persistent organics [3,4]. Titanium dioxide (TiO_2) remains the standard; however, it is constrained by a wide band gap and rapid charge recombination [4,5]. Manganese dioxide has garnered increasing interest as an alternative due to its abundance, low cost, environmental friendliness, natural occurrence in water and sediments, and its role in transforming micropollutants through adsorption and oxidation [6,7]. This review draws exclusively on the papers supplied in the uploaded compilation. Section 2 defines the scope. Sections 3 to 5 treat ciprofloxacin occurrence, adsorptive benchmarks and photocatalytic, electrochemical and singlet-oxygen alternatives. Sections 6 to 9 cover the structure, reactivity and CIP-specific performance of MnO_2 based systems, including MnO_2 carbon composites. Sections 10 to 14 compare mechanisms, kinetics, controlling factors, analytical methods and competing technologies, and Sections 15 to 18 discuss adjacent catalytic applications, practical considerations, a research roadmap and conclusions.

2. SCOPE AND APPROACH

The review is built based on literature papers. They are categorized into six groups in (Table 1). The primary inquiry concerns the extent to which MnO_2 based materials can facilitate the removal of ciprofloxacin from water, as well as the mechanisms involved. Investigations into other pollutants, such as acetaminophen, dyes, methotrexate, and nalidixic acid, are referenced when they provide insights into MnO_2 surface chemistry and the formation of reactive species, as these processes are likely applicable to ciprofloxacin. Quantitative values are presented as reported by the original authors under their specific experimental conditions and should be considered indicative rather than directly comparable.

(This work is licensed under a Creative Commons Attribution 4.0 International License.)

International Journal of Engineering Research & Technology (IJERT)
ISSN: 2278-0181
Vol. 15 Issue 10 , October - 2026

TABLE 1. MAP OF THE SOURCE DOCUMENTS BY TOPIC GROUP.

Group	Source papers	Contribution to this review
A. CIP occurrence, risk, resistance	[1,2, 10]	Concentrations, ecological risk, ARGs, clinical resistance
B. Adsorption of CIP and isotherm theory	[10–14]	Benchmark capacities, mechanisms, modelling
C. Antibiotic photocatalysis, AOPs, $^1O_2$	[3,4, 15–18]	Heterojunctions, reactive species, pathways, toxicity
D. MnO2 materials and reactivity	[6–9, 19–26]	Polymorphs, band gaps, dark and photo-enhanced oxidation
E. Mn-based CIP degradation	[27–30]	Direct CIP performance, PMS activation
F. Adjacent catalysis	[5, 31–38]	Design lessons: supports, doping, immobilisation

3. CIPROFLOXACIN IN THE ENVIRONMENT: OCCURRENCE, RISK AND RESISTANCE

CIP is characterized by its persistence, stability, and widespread use, leading to its accumulation in aquatic environments. Incomplete degradation of CIP can facilitate the development of resistant strains [10, 11]. Data collected from Hong Kong indicate seasonal fluctuations in the levels of CIP and clarithromycin over a 16-month period (December 2019–April 2021), as well as the persistence of antibiotic resistance genes (ARGs) such as acrB-1, acrA-2, mexF, acrA-1, and mexE, in conjunction with CIP- and clarithromycin-resistant bacteria [1]. The same study demonstrated that a PbO_2 thin-film anode effectively removed CIP and clarithromycin within fifteen minutes via electron transfer and reactive oxygen species, highlighting the potential of rapid oxidative treatment to reduce ARG pressure [1].

The clinical aspect is just as significant. With ROC-AUC values of 0.737 (species-agnostic) and 0.837 (species-aware), an ensemble machine-learning model trained on 10,053 cultures from hospitalized patients predicted CIP resistance, identifying prior resistance, patient origin, and recent hospital resistance frequencies as the key predictors [2]. This paper highlights the importance of environmental release of fluoroquinolones because resistance already jeopardizes treatment, even though it does not address water treatment.

4. ADSORPTIVE REMOVAL: THE BENCHMARK

Adsorption is the most intensively studied route for CIP. A systematic review and meta-analysis of studies published between 1990 and 2020 found that CIP adsorption data are generally best described by the Langmuir isotherm and pseudo-second-order kinetics, with optimum pH mostly between 6 and 8.5, a pooled mean removal efficiency of 59.32% (95% CI 44.66–73.97), and a maximum capacity of 1575 mg g−1 for carbon@silica core/shell nanoparticles derived from ZIF-8 [11]. Selection of isotherm models (Langmuir, Freundlich and multi-parameter forms) and appropriate fitting criteria is itself an important methodological issue [12].

The mechanisms are demonstrated by adsorbents based on carbon and clay. With maximal capacities of 379 and 240 mg g^{-1}, graphene oxide (GO) sorbed CIP and sulfamethoxazole. The uptake of CIP was primarily controlled by electrostatic attraction, whereas the uptake of sulfamethoxazole was controlled by π–π electron-donor–acceptor interaction; sorption was significantly influenced by pH and ionic strength (NaCl, $CaCl_2$) [13]. After four cycles, a magnetic chitosan-grafted GO composite maintained roughly 72% of its capacity, reached 282.9 mg g^{-1} (pseudo-second-order kinetics), was repressed by Na^+ and Ca^{2+}, and was regulated by electrostatic and π–π interactions [14]. According to a review of clay-based adsorbents, chemisorption predominates, removals up to roughly 90% are possible, and clay–metal-oxide composites function better than virgin clays [10].

Capacity is sensitive to pH and competing ions, and adsorption moves CIP to a solid phase without destroying it [11, 13, 14]. Destructive methods and hybrid adsorption–catalysis materials, as the BiOX/GaMOF heterojunction, are motivated by this. Adsorption alone removed 50.42% of CIP in 60 minutes, and subsequent irradiation increased removal to 96.27% [16].

The capacity of reported adsorption performance ranges from 47 ng g^{-1} for birnessite to 1575 mg g^{-1} for the best carbon@silica material, spanning over nine orders of magnitude [11]. Additionally, the meta-analysis finds typical enthalpy changes between −1212.6 and +170.21 kJ mol^{-1} and operating temperatures between 273 and 388 K, demonstrating that both exothermic and endothermic absorption occur depending on the adsorbent [11]. To enhance performance, the authors suggest hybrid procedures, neural-network modelling, composite adsorbents, and adsorbent modification [11].

TABLE 2. REPRESENTATIVE ADSORPTION BENCHMARKS FOR CIPROFLOXACIN.

Adsorbent / dataset	Capacity or removal	Notes	Ref.
Carbon@silica core/shell (from ZIF-8)	1575 mg g^{-1} (maximum reported)	Best performer in the meta-analysis	[11]
Birnessite (δ-MnO_2-type)	47 ng g^{-1} (minimum reported)	Lowest capacity in the meta-analysis	[11]
All adsorption studies (pooled)	59.32% mean removal (95% CI 44.66–73.97)	Langmuir and pseudo-second-order fits; pH 6–8.5	[11]
Graphene oxide	379 mg g^{-1} (CIP)	Electrostatic attraction; sensitive to pH, Na^+, Ca^{2+}	[13]
Magnetic chitosan–GO	282.9 mg g^{-1}	Pseudo-second-order; ~72% capacity after four uses	[14]
Clay–metal-oxide composites	Up to ~90% removal	Chemisorption predominant	[10]
BiOX/GaMOF (BG-15)	50.42% in 60 min (dark)	Lewis-acidic Ga, large MOF surface area	[16]

Two aspects of these data are pertinent to the subsequent analysis of MnO_2. Firstly, the surface-charge dependence of CIP uptake, characterized by electrostatic attraction in GO and suppression by competing cations, foreshadows the pronounced pH sensitivity of MnO_2 oxidation, which similarly initiates with adsorption [13, 14, 24]. Secondly, even the least effective MnO_2 type material in the adsorption dataset, birnessite, exhibits negligible capacity, indicating that MnO_2 is not a prominent

(This work is licensed under a Creative Commons Attribution 4.0 International License.)

International Journal of Engineering Research & Technology (IJERT)
ISSN: 2278-0181
Vol. 15 Issue 10 , October - 2026

adsorbent for CIP; its significance lies in oxidative transformation rather than storage [11].

5. PHOTOCATALYTIC, ELECTROCHEMICAL AND SINGLET-OXYGEN ROUTES TO ANTIBIOTIC REMOVAL

5.1 Semiconductor photocatalysis

The application of visible-light photocatalysis to ciprofloxacin (CIP), norfloxacin, tetracyclines, and sulfonamides has been systematically reviewed, focusing on strategies such as doping, heterojunction construction, and surface plasmon resonance to enhance light absorption and inhibit recombination [3]. TiO_2 based systems have been evaluated for the degradation of sulfamethoxazole, trimethoprim, and CIP under various conditions, including catalyst loading, pH, light source, inorganic ions, natural organic matter, and oxidants, with additional criteria being the mineralization and ecotoxicity of the resulting products [4]. The modification of TiO_2 with carbon or transition metals demonstrates the potential of band-gap and charge-separation engineering to enhance photocatalytic activity. For instance, TiO_2 graphene composites achieved over 90% decomposition of perfluorooctanoic acid (PFOA), compared to 16% with commercial TiO_2 [5]. Additionally, Fe- and Ni-doped TiO_2 have been synthesized for the degradation of dyes [37].

Recent examples specific to CIP, as illustrated in Table 3, demonstrate the enhancement of performance through heterojunctions and carbon supports. ZnO nanorods, when decorated on GO, achieved a degradation of 99% of 10 ppm CIP within 75 minutes under sunlight, and 98% of methylene blue within 65 minutes. This outcome is attributed to the presence of oxygen vacancies and OH radicals [17]. A sandwich-like $CuFe_2O_4$/rGO/halloysite catalyst, with a surface area of 130 m^2 g^{-1} and a band gap of approximately 1.9 eV, facilitated nearly complete conversion of 20 ppm CIP in approximately 1 hour, following pseudo-first-order kinetics, with OH radicals and holes serving as the primary active species [18]. The BiOX/GaMOF S-scheme heterojunction integrated adsorption with OH, h^+, O_2^-, and $^1O_2$ pathways, thereby reducing both the predicted and measured toxicity of the products [16].

5.2 Singlet oxygen and fluoroquinolone selectivity

A recent review of singlet oxygen ($^1O_2$) based oxidation indicates that fluoroquinolones generally undergo reactions with $^1O_2$ following second-order kinetics. The review highlights that $^1O_2$ provides selectivity and resistance to matrix interference. The primary reaction pathways include the oxidation of the piperazine ring, decarboxylation, and oxidation of the quinolone moiety, as well as the oxidation of cyclopropyl/oxazinyl substituents. Notably, products resulting from decarboxylation and quinolone oxidation exhibit the lowest predicted toxicity [15]. Given that MnO_2 systems produce $^1O_2$ (as discussed in Section 10), this literature offers a framework for interpreting MnO_2-derived ciprofloxacin (CIP) products [6, 26, 29].

5.3 Electrochemical oxidation as a comparator

Electrochemical oxidation serves as a valuable non-photocatalytic benchmark. In the Hong Kong study, a PbO_2 thin-film anode was electrodeposited from an electrolyte composed of 0.5 mol L^{-1} Pb $(NO_3)_2$, 0.1 mol L^{-1} HNO_3, and 0.02 mol L^{-1} NaF at a current density of 45 mA cm^{-2} for 60 minutes. This anode was utilized in a 200 mL cell with an electrode spacing of 2 cm and a 0.05 mol L^{-1} Na_2SO_4 electrolyte. The stability of the system was assessed using SEM, EDS both before and after 2.5 hours and ten treatment cycles [1]. Hydroxyl and sulfate radicals, along with direct electron transfer, facilitated the removal of CIP and clarithromycin within fifteen minutes. The authors attribute the rapid elimination of antibiotics to the reduction of ARG contamination [1]. Although electrochemical methods achieve removal rates that surpass most photocatalytic systems, which typically require tens of minutes to hours, they necessitate the use of electrodes, an electrolyte, and electrical energy. Additionally, the long-term safety of lead-based anodes must be considered [1].

TABLE 3. REPRESENTATIVE CIPROFLOXACIN (CIP) REMOVAL SYSTEMS DRAWN FROM THE SOURCE PAPERS.

System	Conditions / target	Main result	Dominant species	Ref.
ZnO/GO (GOZ-10)	Sunlight; CIP 10 ppm	99% in 75 min	OH; O vacancies	[17]
$CuFe_2O_4$/rGO/halloysite	Light; CIP 20 ppm; neutral pH	Near-complete in ~1 h; pseudo-first-order	OH, h^+	[18]
BiOX/GaMOF (BG-15)	Adsorption then light, 60 min	50.42% adsorbed; 96.27% total	OH, h^+, O_2^-, $^1O_2$	[16]
Mn/Co oxide (sol–gel)	Sunlight; pH 4; 80 mg catalyst; 0.01 mM CIP	k = 7.9 × 10−2 min^{-1}; photocatalysis > photolysis	Scavenging: ethanol and DMSO strongly inhibit	[27]
γ-Fe_2O_3–MnO_2 / PMS	Visible light, PMS	98.3% in 30 min; k = 0.114 min^{-1}	Radical and non-radical	[30]
α-MnO_2 / PMS	Hydrothermal nanoflowers, nanorods, nanoparticles	Activity: flowers > rods > particles > commercial	SO_4^-, OH; 11 products	[28]
ε-MnO_2 / PMS	Multiple antibiotics incl. CIP; pH 3.5–9.0	ε > α, β, δ-MnO_2	SO_4^-, OH_2, O^-, $^1O_2$; Mn(III)/Mn(IV)	[29]

6. MANGANESE DIOXIDE: STRUCTURE, BAND GAP AND SYNTHESIS

MnO_2 is composed of MnO_6 octahedra, which can connect to form various structural types: tunnel structures (α-, β-, γ-MnO_2), layered structures (δ-MnO_2, birnessite-type), and the three-dimensional ε-form. These one-, two-, and three-dimensional frameworks exhibit differences in surface area, defect density, and Mn (III)/Mn (IV) ratio, which can be adjusted through doping, morphology, and facet control [7, 9]. As a photocatalyst, MnO_2 possesses a narrow band gap of approximately 1–2 eV, enabling response to visible and infrared light. However, its effectiveness is limited by agglomeration, rapid recombination, and low activity at low temperatures. These limitations can be mitigated by forming composites with carbon materials [8, 9]. Common synthesis methods include hydrothermal, sol–gel, precipitation, and reflux techniques [9].

(This work is licensed under a Creative Commons Attribution 4.0 International License.)

International Journal of Engineering Research & Technology (IJERT)
ISSN: 2278-0181
Vol. 15 Issue 10 , October - 2026

The reported optical properties of MnO_2 exhibit significant variation depending on the polymorph and synthesis method employed (Table 5). Specifically, δ-MnO_2 atomic sheets, when laser-crystallized and sonochemically exfoliated, demonstrate band gaps of 1.64 eV and 1.45 eV, respectively [19]. In contrast, δ-MnO_2 nanostructures synthesized via the polyol method exhibit band gaps of 3.02 eV, 2.53 eV, and 2.45 eV, contingent upon the precursor ratio used [21]. Furthermore, the introduction of Ni doping reduces the band gap of MnO_2 nanostructures from 2.78 eV to 1.74 eV and transforms ε-phase flowers into α/β nanowires [22]. These variations underscore the necessity of considering MnO_2 as a collection of distinct materials rather than a singular entity.

Table 4 provides a summary of the structural classes. α-MnO_2 features (2 × 2) tunnels capable of accommodating K^+, Na^+, Ba^{2+}, Mg^{2+}, Ca^{2+}, and water, which is believed to enhance its adsorption capacity. In contrast, β-MnO_2 possesses narrow (1 × 1) tunnels that permit only small ions such as H^+ or Li^+ and exhibits relative stability. γ-MnO_2 is characterized by an intergrowth of tunnel motifs, whereas δ-MnO_2 is a layered material of the birnessite type [7, 23]. Additionally, morphology, including forms such as nanorods, nanotubes, nanowires, nanofibers, nanoribbons, nanosheets, and nanoflowers, influences accessible surface area and defect density. Notably, activity rankings may vary between morphologies even within the same phase [7].

TABLE 4. STRUCTURAL CLASSES OF MnO_2 AND REACTIVITY EVIDENCE FROM THE SOURCE PAPERS.

Polymorph	Dimensionality / structure	Features relevant to oxidation	Ref.
α-MnO_2	1D, (2 × 2) tunnels, tetragonal	Cation- and water-hosting tunnels; strong PMS activation as nanoflowers; wire-like α-MnO_2 reported as most active SO_4^- generator	[7, 28]
β-MnO_2	1D, (1 × 1) tunnels, tetragonal	Stable, narrow tunnels, limited ion diffusion; flower-like β-MnO_2 formed in situ is an effective UV photocatalyst	[6,7]
γ-MnO_2	Intergrown tunnel structure	Larger surface area and weaker electrostatic repulsion favour acidic-pH oxidation	[7, 23]
δ-MnO_2	2D layers (birnessite-type)	High catalytic potential at neutral pH; fastest in sunlight/MnO_2 methotrexate and dye tests	[20, 23, 26]
ε-MnO_2	Hexagonal, cation-vacant (as reported)	High surface – OH content and area; best PMS activator of four polymorphs	[7, 29]

The provided studies demonstrate the variety of preparation techniques and the resulting diversity of materials. These include the hydrothermal growth of α-, β-, γ-, and δ-MnO_2 [20, 28], the reduction of $KMnO_4$ with ascorbic acid for α-MnO_2 and similar methods for β- and δ-forms [26], thermal treatment for ε-MnO_2 [29], polyol synthesis of δ-MnO_2 nanostructures [21], co-precipitation for Ni-doped MnO_2 [22], bottom-up laser crystallization of aqueous $KMnO_4$ and top-down sonochemical exfoliation for δ-MnO_2 atomic sheets [19] sol gel synthesis for Mn/Co oxide [27] and in-situ formation of colloidal MnO_2 through permanganate reduction in water treatment [6]. As each method produces a distinct phase, surface area, defect content, and Mn (III)/Mn (IV) ratio, it is essential to consider the synthesis route when interpreting reported activities.

TABLE 5. STRUCTURE–PROPERTY OBSERVATIONS FOR MnO_2 POLYMORPHS AND COMPOSITES

Material	Key property reported	Ref.
δ-MnO_2 atomic sheets	Band gap 1.64 / 1.45 eV (laser vs. sonochemical route); Raman peaks at 173 and 634 cm^{-1}	[19]
δ-MnO_2 nanostructures (polyol)	Band gap 3.02, 2.53, 2.45 eV; >50% Congo red degraded in 5 min	[21]
α-, β-, γ-, δ-MnO_2 (hydrothermal)	δ-MnO_2 gives 90.4% methylene blue conversion in 180 min; high Mn^{4+}/Mn^{3+}, 2D morphology, lower Mn-O strength	[20]
Ni-doped MnO_2	Band gap 2.78 → 1.74 eV; ε → α/β phase change	[22]
MnO_2-carbon composites	Carbon supports counter agglomeration and low activity	[8]

A comparative analysis of dye photodegradation revealed that δ-MnO_2 exhibits the highest activity, attributed to its strong adsorption of methylene blue, distinctive two-dimensional morphology, weaker Mn-O bonds, and elevated surface Mn^{4+}/Mn^{3+} ratio [20]. These characteristics adsorption, defects, and mixed valence are consistently observed in all MnO_2 reactivity studies discussed herein.

7. MNO_2 CARBON COMPOSITES FOR ANTIBIOTIC REMOVAL

Historically, pristine MnO_2 was regarded as an ineffective photocatalyst for water treatment due to its propensity to agglomerate and its low activity at reduced temperatures. However, its combination with carbon materials, such as graphene, reduced graphene oxide, graphitic carbon nitride, and activated carbon, addresses these limitations and has positioned MnO_2 carbon photocatalysts as a focal point of research [8]. Hydrothermal synthesis is predominantly employed due to water's cost-effectiveness and benign nature, alongside the closed, high-temperature, high-pressure conditions that facilitate intimate MnO_2 carbon interaction and enhance electron transfer. Notable examples include α-MnO_2, RGO nanocomposites, where one-dimensional MnO_2 rods are supported on reduced graphene oxide [8].

The review, as summarized in Table 6, indicates that tetracycline removal rates range from 80% to 97% within 30 to 120 minutes under visible or UV irradiation. Notably, a pumice-supported rGO/MnO_2 solid photocatalyst (PS@rGO@MnO_2) achieved an 80% degradation of ciprofloxacin (CIP) within 6 hours under simulated sunlight. This photocatalyst maintained its performance over three cycles, demonstrated comparable efficacy under real sunlight and in natural water, and was effective against other antibiotics as well [8]. Additionally, the g-C_3N_4/MnO_2/GO heterojunction removed up to 91.4% of tetracycline hydrochloride within 60 minutes and exhibited only a 10% reduction in activity after four cycles, without any structural changes [8]. Although these findings are secondary evidence, as they are reported by the review rather than the

(This work is licensed under a Creative Commons Attribution 4.0 International License.)

International Journal of Engineering Research & Technology (IJERT)
ISSN: 2278-0181
Vol. 15 Issue 10 , October - 2026

primary sources, they suggest that carbon MnO_2 heterojunctions are a promising design for the removal of fluoroquinolones and tetracyclines.

TABLE 6. MnO_2 CARBON PHOTOCATALYSTS FOR ANTIBIOTICS, AS SUMMARIZED IN THE REVIEW OF FAN ET AL.

Photocatalyst	Target (initial conc.)	Light; dose; time	Removal	Ref.
Porous Z-scheme MnO_2/Mn-modified alkalinised g-C_3N_4	Tetracycline (10 mg L^{-1})	Visible, 300 W Xe; 50 mg; 120 min	96.7%	[8]
Carbon nanosheet/MnO_2/BiOCl	Tetracycline HCl (20 mg L^{-1})	UV, 300 W Hg; 20 mg; 30 min	80%	[8]
g-C_3N_4/diatomite/MnO_2	Tetracycline HCl (50 mg L^{-1})	Visible; 30 mg; 60 min	87%	[8]
g-C_3N_4/MnO_2/GO (CMG-10)	Tetracycline HCl (10 mg L^{-1})	Visible, 300 W Xe; 50 mg; 60 min	91.4%	[8]
Pumice-supported rGO/MnO_2	Ciprofloxacin	Simulated sunlight; 6 h	80%; reusable over 3 cycles	[8]

The review acknowledges several limitations associated with MnO_2 carbon composites. These composites typically achieve only 80 to 90% removal efficiency. Additionally, powdered catalysts present challenges in terms of even dispersion and recovery. There is also a risk of adsorbed contaminants being released into the environment during recycling. Furthermore, transitioning from laboratory conditions to real water bodies poses a significant challenge. The review suggests optimizing the MnO_2 carbon ratio, incorporating metal or non-metal dopants, adding polymers or oxides, and developing higher-dimensional structures that are easily separable [8].

8. DARK AND LIGHT-DRIVEN TRANSFORMATION OF PHARMACEUTICALS ON MNO_2

8.1 Dark oxidation and the role of pH and phase

Acetaminophen serves as an effective probe for assessing MnO_2 reactivity. At neutral pH, layered δ-MnO_2 exhibited a faster removal rate compared to tunnel γ-MnO_2, attributed to its superior catalytic potential. Conversely, γ-MnO_2 demonstrated a higher removal rate in acidic conditions due to its larger surface area and reduced electrostatic repulsion. The primary pathways involved were dimerization and hydrolysis oxidation, with acidic pH mitigating the environmental risk of the products [23]. Mechanistically, adsorption played a significant role under acidic conditions but was negligible at neutral and alkaline pH levels. Consequently, electron transfer was the rate-limiting step in acidic media, while precursor-complex formation limited the rate in neutral and alkaline conditions. The kinetics were characterized by surface-complexation, Michaelis Menten, or pseudo first order models, contingent on the loading [24]. For δ-MnO_2, optimal removal was achieved at a high dose (800 mg L^{-1}), 50 °C, and pH 3.0 to 3.5, involving an endothermic reaction with dimer/trimer intermediates that were subsequently consumed [25].

8.2 Photo-enhanced transformation

Light alters the image. With pseudo-first-order constants of 0.299 and 0.116 min^{-1}, freshly formed colloidal MnO_2 (flower-like β-MnO_2) removed nalidixic acid and gemfibrozil under UV, outperforming commercial MnO_2 due to superior adsorption; EPR detected OH, O^-, and O_2^- VB-XPS and UV–vis results showed that ROS arise solely from electron reaction with oxygen, with holes dominating nalidixic acid oxidation [6]. The closest analogue to CIP in the provided MnO_2 photocatalysis literature is nalidixic acid, which is a quinolone in and of itself.

Every polymorph was accelerated by light since methotrexate degradation by α-, β-, and δ-MnO_2 followed pseudo-first-order kinetics under simulated sunlight, with rate constants of 4.6, 6.4, and 7.3 × 10−3 min^{-1}, greater than in the dark (1.6, 1.8, and 6.0 × 10−3 min^{-1}) [26]. Photolysis dominated for α- (55.6%) and β-MnO_2 (40.3%), while MnO_2 oxidation dominated for δ-MnO_2 (about 70.1%), according to a contribution analysis that divided removal among photolysis, MnO_2 oxidation, and reactive manganese species (RMnS); XPS identified Mn (III) as the primary RMnS, and EPR verified O^- and $^1O_2$ in both dark and sunlight systems [26]. This partition serves as a helpful CIP template, which also undergoes direct photolysis.

9. MN-BASED SYSTEMS THAT DEGRADE CIPROFLOXACIN

9.1 Photocatalysis with Mn/Co oxide

A sol–gel Mn/Co oxide degraded CIP under sunlight faster than photolysis alone (k = 7.9 × 10^{-2} min^{-1}), with best activity at pH 4, high catalyst dose (80 mg) and low CIP concentration (0.01 mM); scavenger tests showed that ethanol and DMSO strongly suppressed the reaction, implicating radical species [27]. This is the only study in the compilation in which a pristine Mn oxide based photocatalyst is applied to CIP under sunlight.

9.2 MnO_2-activated peroxymonosulfate

More research has been done on MnO_2's ability to activate PMS. Tracking specific surface area and crystallinity, hydrothermal α-MnO_2 nanoflowers, nanorods, and nanoparticles triggered PMS for CIP degradation in the following order: flowers, rods, particles, commercial MnO_2. Eleven oxidation products were found; piperazine-ring cleavage, hydroxylation, and F/OH substitution were the main pathways; removal was favored in acid and accelerated in alkaline media; bicarbonate and chloride had concentration-dependent dual effects; natural organic matter was harmful; and acute toxicity decreased over time [28]. Comparing α-, β-, δ-and ε-MnO_2, the ε-phase activated PMS most efficiently across sulfonamides, CIP and azithromycin because of high surface hydroxyl content, unique structure and large surface area, operating at pH 3.5 to 9.0 through inner-sphere PMS complexation and Mn (III)/Mn (IV) cycling that produced SO_4^-, OH, O_2^- and $^1O_2$ [29].

9.3 Coupling light with PMS activation

Magnetic γ-Fe_2O_3 MnO_2, characterized by adjustable oxygen vacancies through varying the amorphous MnO_2 content, achieved a 98.3% removal of CIP within 30 minutes under visible light/PMS conditions (k = 0.114 min^{-1}). An optimal vacancy density enhanced charge separation, while a Z scheme

(This work is licensed under a Creative Commons Attribution 4.0 International License.)

International Journal of Engineering Research & Technology (IJERT)
ISSN: 2278-0181
Vol. 15 Issue 10 , October - 2026

heterostructure maintained a robust redox potential. Both radical and non-radical pathways were active, and selectivity was preserved despite the presence of co-existing anions. The catalyst demonstrated stability, magnetic recoverability, and reusability [30]. This hybrid system exemplifies an optimal design strategy for MnO_2, wherein the oxide is coupled with a secondary phase that facilitates charge separation or magnetic recovery, while maintaining Mn redox activity.

9.4 Comparative CIP performance and secondary evidence

In addition to the four principal Mn CIP studies, the provided reviews present further findings related to MnO_2 and CIP degradation. Li et al.'s review indicates that α-MnO_2, when combined with dielectric-barrier discharge, achieved a 93.1% degradation of CIP within 50 minutes. Furthermore, copper based bimetallic oxides activated by H_2O_2 attained complete degradation, and wire-like α-MnO_2 was identified as the most active crystalline form for SO_4^- generation [7]. The review on photocatalytic dyes highlights a $MnO_2/Mn_2O_3/Mn_3O_4$ mixed valence photocatalyst, which removed 95.6% of CIP in 40 minutes under visible light, with an optimal pH of 7 within the tested pH range of 4 to 10 [9]. Table 7 places these alongside the primary studies.

TABLE 7. MN BASED CIPROFLOXACIN REMOVAL SYSTEMS, PRIMARY AND SECONDARY EVIDENCE.

Mn system	Process	Key conditions	Result	Ref.
Mn/Co oxide (sol–gel)	Sunlight photocatalysis	pH 4; 80 mg; 0.01 mM CIP	k = 7.9 × 10−2 min−1	[27]
γ-Fe_2O_3–MnO_2	Visible light + PMS	Oxygen-vacancy tuned	98.3% / 30 min; k = 0.114 min−1	[30]
α-MnO_2 nanoflowers	PMS activation	Acidic or alkaline pH	Best of four α-morphologies; 11 products	[28]
ε-MnO_2	PMS activation	pH 3.5–9.0	Best of α, β, δ, ε	[29]
$MnO_2/Mn_2O_3/Mn_3O_4$	Visible photocatalysis	pH 7 optimum	95.6% / 40 min (secondary)	[9]
α-MnO_2 + DBD	Plasma	—	93.1% / 50 min (secondary)	[7]
PS@rGO@MnO_2	Simulated sunlight	3 reuse cycles	80% / 6 h (secondary)	[8]

The table shows that light, oxidant or plasma coupling is generally needed to reach greater than 90% CIP removal within an hour; none of the supplied studies reports a stand-alone, dark MnO_2 oxidation of CIP of comparable speed. A fair interpretation is that MnO_2 alone is a modest CIP oxidant at near-neutral pH, whereas its role as a PMS activator, as a visible-light photocatalyst in a heterostructure, or as a source of reactive Mn (III) in sunlight provides the strong effects.

9.5 Case-study synopses of the primary Mn–CIP studies

α-MnO_2/PMS (Deng et al.). Three α-MnO_2 morphologies were synthesized hydrothermally and evaluated against commercial MnO_2. The activity hierarchy observed was nanoflowers, nanorods, nanoparticles, commercial, primarily influenced by specific surface area and crystallinity. This study is distinguished by its comprehensive examination of water chemistry, including Cl^-, HCO_3^-, and NOM. It employs UPLC–MS/MS to monitor eleven oxidation products, with five exhibiting a consistent increase and four declining post-formation. Additionally, the study assesses acute toxicity, which decreased with treatment progression and increased PMS dosage, and provides fluorescence EEM evidence of functionality within an actual water matrix [28].

ε-MnO_2/PMS (Khan et al.). ε-MnO_2, synthesized through a straightforward thermal treatment, demonstrated superior efficiency in eliminating sulfamethoxazole, sulfachloropyridazine, sulfamethazine, ciprofloxacin, and azithromycin compared to α-, β-, and δ-MnO_2. This enhanced performance is attributed to its high surface hydroxyl content, structural characteristics, and surface area. The process generated sulfate, hydroxyl, and superoxide radicals, as well as singlet oxygen, with superoxide (O_2^-) serving as the $^1O_2$ precursor. The addition of carbonate (10 mM) reduced sulfamethoxazole removal efficiency from 99% to 45%, indicating a significant role for superoxide. The proposed mechanism involves inner-sphere PMS MnO_2 complexation and electron transfer between Mn (III) and Mn (IV). The system operated effectively across a pH range of 3.5 to 9.0, with minimal interference from inorganic anions or natural organic matter (NOM) [29].

γ-Fe_2O_3–MnO_2 (Zhao et al.). The proportion of amorphous-MnO_2 was adjusted to optimize the oxygen-vacancy density, with the 2:1 composite demonstrating superior performance. The Z scheme heterostructure preserved a high redox potential, while the vacancies facilitated charge separation. The synergy between photocatalysis and PMS activation, along with the coexistence of radical and non-radical pathways, accounted for the 98.3% removal efficiency achieved within 30 minutes. Additionally, the catalyst was magnetically recoverable and maintained high selectivity in the presence of anions [30].

Mn/Co oxide (Alam et al.). The sol–gel Mn/Co oxide was characterized using FESEM, XRD, BET, TGA, and diffuse reflectance techniques, and its performance was evaluated under sunlight. The photocatalytic process demonstrated superior efficiency compared to photolysis, with the reaction rate being influenced by pH (optimal at 4), catalyst dosage (80 mg), and CIP concentration (optimal at 0.01 mM). The presence of scavengers such as ethanol and DMSO significantly inhibited degradation. The primary advantage of this system is its reliance solely on sunlight and a simple oxide; however, the study lacks data on product identification, toxicity, and reuse, as indicated in the provided pages [27].

10. MECHANISMS AND TRANSFORMATION PATHWAYS

Figure 1 illustrates a composite mechanism derived from the source studies. Upon photo-excitation, MnO_2 generates electron–hole pairs, where electrons reduce O_2 to O_2^- (and, through subsequent steps, to $^1O_2$ and OH), while holes oxidize CIP directly or water to OH [6,9]. In the presence of PMS, the cycling of surface Mn (III)/Mn (IV) produces SO_4^- and OH, as well as non-radical $^1O_2$ [29,30]. In the absence of light, inner-sphere complexation followed by electron transfer to Mn (IV) results in Mn (III) intermediates, which function as reactive manganese species [24, 26].

(This work is licensed under a Creative Commons Attribution 4.0 International License.)

International Journal of Engineering Research & Technology (IJERT)
ISSN: 2278-0181
Vol. 15 Issue 10 , October - 2026

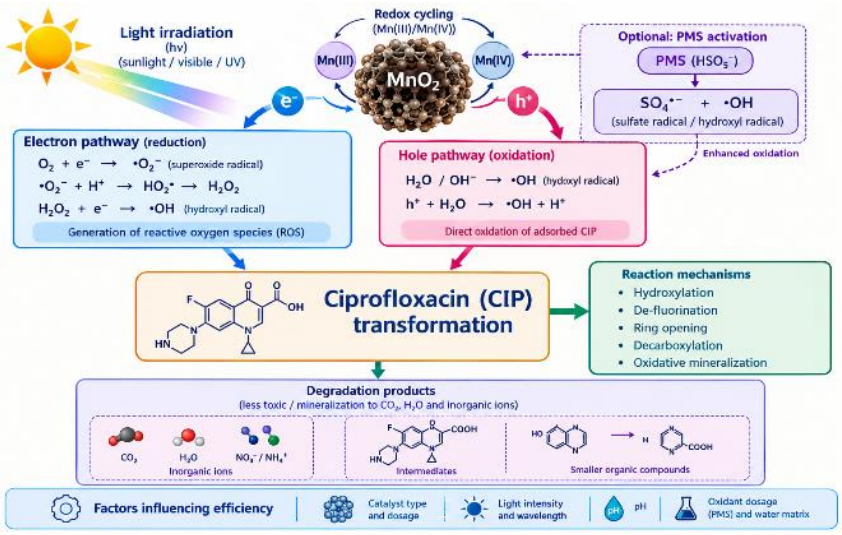


Figure 1. Composite mechanism for MnO_2-based photocatalytic and PMS assisted CIP oxidation, synthesized from [6, 26, 28–30].

Fluoroquinolones undergo transformation through similar pathways across various systems, involving processes such as oxidation or the opening of the piperazine ring, hydroxylation, F/OH substitution, and decarboxylation or oxidation of the quinolone core [15, 28]. The toxicity results are promising but vary depending on the pathway: acute toxicity decreased during α-MnO_2/PMS treatment, with a higher PMS dose enhancing detoxification [28]; photocatalytic treatment using BiOX/GaMOF reduced both predicted and bacterial toxicity [16]; and oxidation products of the quinolone moiety from $^1O_2$ were found to be the least toxic [15]. In the dark oxidation of acetaminophen by MnO_2, an acidic pH lowered the risk associated with the products, although dimerization can lead to larger species that require monitoring [23, 25].

11. KINETICS AND MODELLING

Photocatalytic and oxidative kinetics: Nearly all CIP degradation studies in the literature adhere to pseudo-first-order kinetics, including those involving $CuFe_2O_4$/rGO/halloysite [18], Mn/Co oxide [27], and γ-Fe_2O_3 MnO_2/PMS [30]. This model is also applied to the removal of micropollutants using UV/MnO_2 [6], methotrexate removal with sunlight/MnO_2 [26], and humic acid coated TiO_2 [38]. Table 8 collects the reported constants. Because pseudo-first-order constants depend on catalyst dose, pollutant concentration, light intensity and reactor geometry, they should be compared only qualitatively, or after normalization by catalyst mass, surface area or photon flux.

TABLE 8. REPORTED PSEUDO-FIRST-ORDER RATE CONSTANTS.

System	Pollutant	k (min−1)	Ref.
γ-Fe_2O_3–MnO_2 / visible light / PMS	Ciprofloxacin	0.114	[30]
Mn/Co oxide / sunlight	Ciprofloxacin	7.9 × 10−2	[27]
UV / colloidal MnO_2	Nalidixic acid	0.299	[6]
UV / colloidal MnO_2	Gemfibrozil	0.116	[6]
Humic-acid-coated TiO_2 / LED white light	Bisphenol A	1.7 × 10−2	[38]
Sunlight / δ-MnO_2	Methotrexate	7.3 × 10−3	[26]
Sunlight / β-MnO_2	Methotrexate	6.4 × 10−3	[26]
Sunlight / α-MnO_2	Methotrexate	4.6 × 10−3	[26]
Dark / δ-MnO_2	Methotrexate	6.0 × 10−3	[26]

(This work is licensed under a Creative Commons Attribution 4.0 International License.)

International Journal of Engineering Research & Technology (IJERT)
ISSN: 2278-0181
Vol. 15 Issue 10 , October - 2026

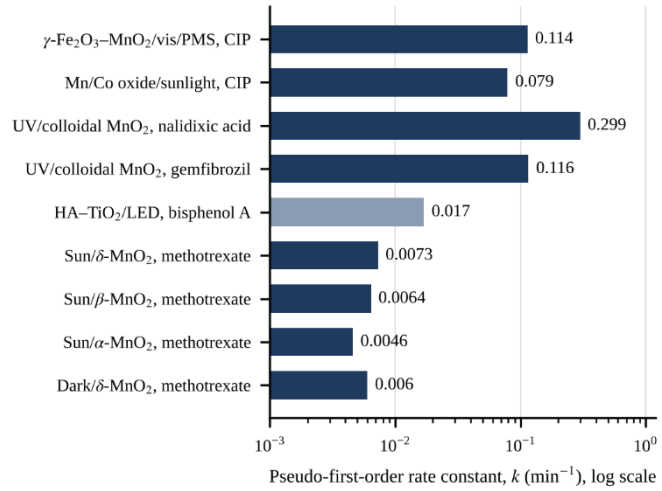


Figure 2. Reported pseudo-first-order rate constants from Table 8 (dark bars: Mn-based systems). Values are from different experimental set-ups and are for qualitative comparison only [6, 26, 27, 30, 38].

Surface-limited kinetics on MnO_2: The kinetics of dark oxidation on MnO_2 do not consistently follow first-order behavior. When acetaminophen is present in amounts greater than the available reactive surface sites, a model based on surface complexation and transformation is applicable. In contrast, acidic conditions are best described by a Michaelis–Menten model, while neutral and alkaline conditions align with a pseudo-first-order model [24]. Analyzing δ-MnO_2 using the Arrhenius equation revealed a positive activation energy, suggesting the reaction is endothermic. The data fit two assumptions regarding the rate-limiting step: either electron transfer or complex formation [25]. This implies that rate constants determined at a specific MnO_2-to-pollutant ratio cannot be generalized to other ratios, explaining why initial concentration effects vary across different polymorphs [26]. For singlet oxygen, fluoroquinolones generally undergo reactions characterized by second-order kinetics, and it has been suggested that listing second-order constants along with reaction pathways could serve as a method for comparing oxidants [15].

Adsorption models: CIP adsorption is typically modeled using Langmuir or Freundlich isotherms and follows pseudo-second-order kinetics [11, 14]. An examination of isotherm theory categorizes models based on their parameter count, advises on careful selection criteria, and highlights that while the widely used linear-regression method is straightforward, it can skew parameters. Therefore, non-linear fitting and model-selection statistics are recommended [12]. These considerations are equally relevant to MnO_2 studies, where adsorption initiates surface oxidation.

12. FACTORS GOVERNING PERFORMANCE

pH: Acidic conditions generally enhance MnO_2 oxidation of organics by improving adsorption and limiting electron-transfer oxidation [23–25]. Mn/Co photocatalysis of CIP reached its maximum efficiency at pH 4 [27], whereas ε-MnO_2/PMS was effective across a pH range of 3.5 to 9.0 [29], and α-MnO_2/PMS showed increased activity in alkaline environments [28]. Since CIP is zwitterionic, its speciation affects interactions with the MnO_2 surface charge; the pH-dependent net charge of δ-MnO_2 was found to influence dye degradation [21].

Catalyst dose and pollutant concentration: An increased dose of MnO_2 enhanced the removal of methotrexate across all polymorphs, while the initial concentration of the pollutant had varying impacts on the polymorphs, indicating different mechanisms [26]. A high Mn/Co dose combined with a low CIP concentration promoted CIP removal [27]. However, an excess of catalyst can hinder the degradation of certain dyes, as seen with Congo red, where the trend reversed beyond a 10 mg dose [21].

Water matrix: Chloride and bicarbonate exhibited dual effects dependent on concentration, and natural organic matter inhibited α-MnO_2/PMS [28]. In contrast, ε-MnO_2/PMS was only slightly influenced by inorganic anions and NOM in the case of sulfamethoxazole [29], and γ-Fe_2O_3 MnO_2 maintained high selectivity even with co-existing anions [30]. Fluorescence EEM results showed that α-MnO_2/PMS remained effective in actual water conditions [28].

Crystal phase and morphology: The polymorphs are ranked by surface area, crystallinity, 2D morphology, and defect/vacancy chemistry [20, 28, 30]. Overall, δ-MnO_2 and ε-MnO_2 consistently outperform α- and β-MnO_2 in neutral systems [20, 23, 26, 29], although α-MnO_2 nanoflowers can be potent PMS activators [28].

TABLE 9. SUMMARY OF FACTORS CONTROLLING CIP AND RELATED REMOVAL ON MN-BASED SYSTEMS.

Factor	Observed effect	Ref.
Solution pH	Acid favours MnO_2 oxidation of acetaminophen (δ-MnO_2 optimum 3.0–3.5); Mn/Co–CIP optimum pH 4; ε-MnO_2/PMS works at pH 3.5–9.0; α-MnO_2/PMS accelerated in alkali; $CuFe_2O_4$/rGO/HNT effective at neutral pH	[18, 25, 27–29]
Catalyst dose	Higher dose raises rate (methotrexate, Mn/Co–CIP); reversed for Congo red above 10 mg	[21, 26,27]
Pollutant concentration	Low CIP concentration favoured removal; polymorph-specific effects of initial concentration	[26,27]
Anions (Cl^-, HCO_3^-)	Concentration-dependent dual effects on α-MnO_2/PMS; minor effects on ε-MnO_2/PMS	[28,29]
Natural organic matter	Detrimental for α-MnO_2/PMS; small effect on ε-MnO_2/PMS	[28,29]
Light source and intensity	Sunlight, visible and UV all enhance MnO2 reactions; photolysis contributes strongly for α- and β-MnO_2	[6, 26,27]
Temperature	Positive activation energy; endothermic on δ-MnO_2	[25]
Ionic strength (adsorption)	Na^+ and Ca^{2+} suppress CIP uptake on GO-type sorbents	[13,14]

13. ANALYTICAL AND CHARACTERIZATION METHODS

Credible conclusions regarding MnO_2 CIP chemistry necessitate the integration of materials, analytical, and biological methods, as outlined in Table 10. The characterization of materials through techniques such as XRD, Raman spectroscopy, SEM/TEM, BET, XPS, and UV vis diffuse reflectance with Tauc analysis determines the phase,

(This work is licensed under a Creative Commons Attribution 4.0 International License.)

International Journal of Engineering Research & Technology (IJERT)
ISSN: 2278-0181
Vol. 15 Issue 10 , October - 2026

morphology, surface area, oxidation state, and band gap [19–21]. Reactive species are identified via scavenger experiments, which have implicated OH and species sensitive to DMSO or ethanol in Mn/Co–CIP photocatalysis, and OH in ZnO/GO systems [17, 27]. Additionally, EPR analysis has detected OH, O_2^{-}, and $^1O_2$ in both UV/MnO_2 and sunlight/dark MnO_2 systems [6, 26]. Given that scavengers may react with Mn species and oxidants, it is essential to corroborate findings with both EPR and probe-compound evidence.

TABLE 10. ANALYTICAL AND CHARACTERIZATION TECHNIQUES USED IN THE SOURCE STUDIES.

Technique	Purpose	Examples in source papers
HPLC;UPLC–MS/MS; RPLC–QToF	Quantify CIP; identify intermediates	Environmental sampling [1]; 11 CIP products [28]; acetaminophen dimers/trimers [25]
XRD, Raman, SEM/TEM, BET	Phase, morphology, surface area	MnO_2 polymorphs [20]; δ-MnO_2 sheets [19]; Mn/Co oxide [27]
XPS, valence-band XPS	Mn oxidation state; band edges	Mn(III) as RMnS [26]; ROS formation pathway [6]
EPR	Detect OH, O_2^{-} , $^1O_2$	[6, 16, 26]
UV–vis, Tauc plot	Band gap	[21,22]
Scavenger tests	Identify dominant species	[17, 27]
Fluorescence EEM	Behavior in natural water background	[28]
Toxicity prediction; bacterial assays	Product toxicity	[16, 28]
16S rRNA sequencing; ARG profiling	Resistance and microbiome context	[1]
Voltammetry (LSV/CV)	Electrocatalytic performance of Mn oxides	[22, 32]

In the Hong Kong monitoring study, 0.45 µm-filtered water samples were analyzed by HPLC, and the bacterial community was characterized by amplifying the V3–V4 region of the 16S rRNA gene with primers 341F and 806R [1]. Pairing chemical removal data with ARG and community data of this kind is rare in the catalyst literature and would add considerable value to MnO_2–CIP studies.

14. COMPARATIVE ASSESSMENT OF TREATMENT STRATEGIES

Table 11 compares the strategies discussed. Adsorption is robust and simple but non-destructive and pH-sensitive [11, 13]. TiO_2 photocatalysis is mature but limited by a wide band gap and recombination [4, 5]. Heterojunction photocatalysts (ZnO/GO, $CuFe_2O_4$/rGO/HNT, BiOX/GaMOF) give excellent laboratory removal in an hour or less [16–18]. MnO_2 based routes add earth-abundant redox chemistry and a versatile role as PMS activator, and avoid precious metals [28, 29]. Electrochemical oxidation is fast but electrode- and energy-dependent [1], whereas singlet-oxygen oxidation offers selectivity and toxicity reduction but its generation by practical catalysts is still developing [15].

TABLE 11. STRENGTHS AND LIMITATIONS OF CIP TREATMENT STRATEGIES.

Strategy	Strengths	Limitations	Ref.
Adsorption	Simple; wide range of sorbents; high capacities	No destruction; pH and ionic-strength sensitive; regeneration loss	[11, 14]
TiO_2-based photocatalysis	Mature; stable; solar-capable	Wide band gap; recombination; catalyst recovery	[4,5]
Heterojunction photocatalysis (ZnO/GO, BiOX/GaMOF)	Near-complete CIP removal in ~1 h; reduced toxicity	Complex synthesis; Bi/Ga cost; lab-scale	[16,17]
MnO_2 dark oxidation	Earth-abundant; strong at acidic pH	Mn leaching; pH-limited; slow for CIP at neutral pH	[23,24]
MnO_2 photocatalysis / sunlight	Visible response; Mn(III) boost; solar energy	Few CIP-specific studies; recombination; agglomeration	[9, 26,27]
MnO_2/PMS and light/PMS	Radical and non-radical routes; >98% in 30 min	Oxidant cost; sulfate residue; matrix effects	[28–30]
Electrochemical (PbO_2)	CIP removed in 15 min; ARG mitigation	Electrodes, energy, lead-based anode	[1]
$^1O_2$ -based AOPs	Selective; robust to matrix; less toxic products	Generation and detection challenges	[15]

14.1 Integrating the evidence: a framework for selecting MnO_2 systems

Upon reviewing the source literature, three distinct regimes of MnO_2 behavior are identifiable. In the surface-oxidation regime, which occurs under dark or weak illumination and in acidic to neutral pH conditions, reactivity is primarily influenced by adsorption, the reducibility of Mn (IV), and the availability of surface sites. Under these conditions, layered δ-MnO_2 and high-surface-area γ- or ε-forms exhibit optimal performance, and the kinetics are saturable [23–25]. In the photo-enhanced regime, which involves exposure to UV, sunlight, or visible light, photo-generated carriers and Mn (III) augment surface oxidation, and for certain polymorphs, direct photolysis of the pollutant may predominate. The contribution of each pathway in this regime is contingent upon the specific polymorph and pollutant involved [6, 26]. In the oxidant-activation regime, MnO_2 functions as a redox mediator for PMS, with surface hydroxyl groups, Mn (III)/Mn (IV) cycling, and oxygen vacancies playing crucial roles in the production of both radical and non-radical species [28–30].

These regimes suggest a practical decision logic for CIP. Where acidic effluents or pretreatment steps are acceptable, dark MnO_2 may be a low-cost polishing step but should be tested for Mn release. Where sunlight is available, δ-MnO_2 or Mn (III)-rich heterostructures are the most promising candidates, but need CIP-specific verification. Where rapid, matrix-tolerant

(This work is licensed under a Creative Commons Attribution 4.0 International License.)

International Journal of Engineering Research & Technology (IJERT)
ISSN: 2278-0181
Vol. 15 Issue 10 , October - 2026

removal is the goal, MnO_2/PMS or visible-light/PMS systems deliver greater than 95% removal in 30 min in the laboratory, at the price of an added oxidant [29,30].

Discrepancies and open questions. Several results in the corpus are not fully reconciled. α-MnO_2 is the weakest sunlight/MnO_2 polymorph for methotrexate but a strong PMS activator for CIP [26, 28], ε-MnO2 outperforms δ-MnO_2 for PMS activation while δ-MnO_2 is the most active in photocatalytic dye degradation [20, 29] and acid improves most MnO_2 oxidations whereas alkaline conditions accelerate α-MnO_2/PMS [24, 28]. These differences probably reflect different rate-limiting steps (adsorption, electron transfer, oxidant activation, light absorption) and different synthesis routes, rather than inconsistency, and they argue strongly for pollutant-specific testing.

15. LESSONS FROM ADJACENT MNO_2, TIO_2 AND CARBON-COMPOSITE CATALYSIS

The compilation encompasses studies beyond water-phase antibiotic removal, whose design principles are transferable. Pt-loaded MnO_2 nanoarrays on honeycomb cordierite achieved a T_{50} of 189 °C for acetone oxidation with 42 hours of water resistance, indicating that structured, monolithic MnO_2 supports can enhance surface lattice oxygen activity [31]. This finding suggests that immobilized MnO_2 arrays could serve as a pathway to recoverable water catalysts. In the field of electrocatalysis, Ni-doped MnO_2 demonstrated improved oxygen reduction [22]. Additionally, Ni-MnO_2/TiO_2 reached a current density of 10 mA cm−2 at 1.29 V for urea oxidation [32], while PtCu/RGO–TiO_2 exhibited a higher ORR limiting current density (6.14 mA cm−2) compared to Pt/C [33]. Collectively, these results demonstrate that interfacial engineering between MnO_2, TiO_2, and graphene-type supports enhances charge transport.

In the field of water treatment, GO–TiO_2 photoanodes were able to nearly completely decompose 0.5 mg L^{-1} of PFOA within 4 hours, resulting in the identification of 18 transformation products [34]. Similarly, Fe/sulfonated-ZrO_2 achieved full conversion of clofibric acid in 1 hour and 57% mineralization over 6 hours through Fenton-like catalysis, notably without iron leaching [35]. Furthermore, TiO_2 supported on nickel slag increased methylene blue removal efficiency from 48% (via photolysis) to 87.5% (via photocatalysis), highlighting the efficacy of waste-derived supports [36]. These examples underscore three critical design considerations pertinent to MnO_2/CIP: the use of supports or heterojunction partners for effective charge separation, the importance of immobilization for recovery, and the necessity of benchmarking against direct photolysis.

16. PRACTICAL CONSIDERATIONS FOR IMPLEMENTATION

Catalyst separation and reuse: Powder catalysts exhibit uneven dispersion and pose challenges in recovery, with quantitative losses during recycling potentially affecting the fate of adsorbed contaminants [8]. Potential solutions include magnetic separation (γ-Fe_2O_3 MnO_2) [30], immobilization on structured supports such as MnO_2 nanoarrays on cordierite honeycombs and pumice-supported rGO/MnO_2 [8, 31], and the use of waste-derived supports like nickel slag [36].

Stability, leaching and safety: A review of visible-light antibiotic photocatalysts highlights that most research is conducted at the laboratory scale, the removal of photocatalysts from treated water remains insufficiently studied, material stability and reusability at larger scales present significant challenges, and only a limited number of studies evaluate material safety in animal models [3]. For MnO_2, the reduction of Mn (IV) during oxidation necessitates monitoring of dissolved Mn and the stability of reduced phases in every study.

Energy and light: Sunlight-driven demonstrations, such as those involving Mn/Co oxide, ZnO/GO, and pumice-supported rGO/MnO_2, facilitate low-energy operations [8, 17, 27]. Conversely, LED white light presents an energy-efficient alternative for catalysts responsive to visible light [38]. Photoreactors utilizing MnO_2 must address the challenge of light penetration in colored or turbid water, a well-documented limitation of heterogeneous photocatalysts [16].

Water matrix and mixtures: Real wastewater comprises chloride, bicarbonate, natural organic matter, and numerous co-contaminants that compete for oxidants or surface sites [4, 28]. Studies focusing on dyes often employ single, relatively easy-to-remove model pollutants, which may result in high efficiencies that do not necessarily translate to complex effluents [9].

Resistance endpoints: Given that the motivation for ciprofloxacin (CIP) removal includes resistance control, treatment studies should report not only the removal of the parent compound but also the residual antibacterial activity and, where feasible, the reduction of antibiotic resistance genes (ARG) and resistant bacteria [1, 16].

17. CHALLENGES AND RESEARCH ROADMAP

Evidence gap for pristine MnO2 photocatalysis of CIP: Among the studies provided, only one employs a Mn-oxide photocatalyst directly on CIP under light conditions without an oxidant [27]; the others utilize PMS, UV on different quinolones, or other pollutants [6, 28–30]. It is necessary to conduct controlled comparisons of α-, β-, γ-, δ-, and ε-MnO_2 for CIP under identical light, pH, and matrix conditions, ideally employing the photolysis/MnO_2 oxidation/RMnS partitioning method used for methotrexate [26].

Stability and Mn leaching: The reduction of Mn(IV) to soluble Mn(II) during oxidation limits the catalyst's lifespan and raises concerns regarding effluent quality; therefore, stability, reuse, and metal leaching should be routinely reported, as demonstrated in the magnetic γ-Fe_2O_3–MnO_2 study [30]. Carbon and magnetic supports present promising solutions [8, 30].

Real waters, mixtures and toxicity: Most studies on MnO_2 employ model dyes or single pollutants at concentrations significantly exceeding environmental levels (ng L−1 to µg L−1 [1]). It is crucial to conduct tests in actual effluent, incorporating mixtures and endpoints such as antibiotic resistance genes (ARG) and antibiotic-resistant bacteria [1, 9]. Standard procedures should include product identification, mineralization, and ecotoxicity assessment [4, 15].

Hybrid and scalable designs: Promising research directions encompass MnO_2 carbon composites [8], S-scheme or Z-scheme heterojunctions with metal-organic frameworks (MOFs) or oxides [16, 30], doping to reduce the band gap [22], immobilized nanoarrays [31], and the integration of adsorption

(This work is licensed under a Creative Commons Attribution 4.0 International License.)

International Journal of Engineering Research & Technology (IJERT)
ISSN: 2278-0181
Vol. 15 Issue 10 , October - 2026

and catalysis to concentrate ciprofloxacin (CIP) at the active surface [11, 16]. Machine-learning tools, which are already employed to predict CIP resistance in clinical settings [2], could potentially be utilized in the future to screen catalysts and determine optimal operating conditions.

17.1 Materials design

Design priorities are derived from structure–activity evidence, emphasizing the control of polymorph and defect chemistry, specifically δ- and ε-MnO_2 with controlled oxygen vacancies [20, 29, 30]. Additionally, narrowing the band gap through doping or heterostructure formation is crucial, as demonstrated by Ni doping, which reduced the gap from 2.78 to 1.74 eV [22]. Furthermore, coupling MnO_2 with conductive or charge-separating partners, such as rGO, g-C_3N_4, ferrites, or MOFs, in Z-scheme or S-scheme arrangements, is recommended [8, 16, 30]. The design of heterojunctions in the BiOX/GaMOF and γ-Fe_2O_3–MnO_2 systems serves as templates for the necessary interfaces [16, 30].

17.2 Mechanistic understanding

Mechanistic studies should quantify the contributions of direct photolysis, surface MnO_2 oxidation, Mn(III)-mediated oxidation, and reactive oxygen species (ROS) for CIP, as has been done for methotrexate [26]. It is also essential to clarify the origin of singlet oxygen (whether as a precursor of O_2^- or through direct energy transfer) [6, 29], and to map CIP transformation pathways with product toxicity, linking them to the pathway types identified for singlet-oxygen oxidation [15, 28].

17.3 Process engineering and risk

Key priorities encompass the utilization of continuous-flow or monolithic reactors employing supported MnO_2 [31], alongside conducting life-cycle and cost assessments in comparison to TiO_2 and adsorption alternatives [4, 11]. Additionally, the integration with biological treatment or adsorption processes is considered. Machine-learning methodologies, which have been successfully applied to predict clinical CIP resistance, may be adapted to forecast catalyst performance based on synthesis and operational variables [2].

TABLE 12. PROPOSED RESEARCH ROADMAP DERIVED FROM THE GAPS IDENTIFIED IN THIS REVIEW.

Priority	Gap identified	Suggested study	Basis
1	Few light-driven CIP studies on pristine MnO_2 polymorphs	Compare α-, β-, γ-, δ-, ε-MnO_2 for CIP under identical light, pH and dose; partition photolysis, MnO_2 oxidation and RMnS	[26,27]
2	Mechanism of Mn (III) and ROS formation with CIP	XPS, EPR and probe experiments; isotopic or competition tests	[6, 26]
3	Stability, Mn leaching and reuse	Multi-cycle tests with dissolved-Mn and phase-stability analysis	[3, 30]
4	Catalyst recovery and scale-up	Magnetic, supported or monolithic MnO_2; pilot flow reactors	[8, 30,31]
5	Real water and mixtures	Test in effluent, river water and with co-contaminants at ng–μg L−1	[1, 9]
6	Toxicity and resistance outcomes	Product toxicity, antibacterial activity, ARG tracking	[1, 16, 28]
7	Standardized reporting	Normalized rate constants, photon flux, control experiments, non-linear model fitting	[12, 26]

18. CONCLUSIONS

CIP is a persistent micropollutant associated with resistance, which cannot be effectively removed through adsorption alone. MnO_2 serves as an appealing, cost-effective oxidant and photocatalyst, with its reactivity being influenced by its polymorph, defect state, and pH-dependent surface chemistry. Among these, δ- and ε-MnO_2 are often the most reactive. The presence of light, PMS, or both induces the formation of a mixture of h^+, OH, SO_4^-, O_2^-, $^1O_2$, and Mn (III) species. These species facilitate the opening of the piperazine ring, hydroxylation of the molecule, and displacement of fluorine, typically resulting in reduced toxicity. Future advancements require systematic studies of polymorphs for CIP under light, the development of durable and recoverable composite designs, and validation in real water environments with a focus on toxicity and resistance endpoints.

REFERENCES

[1] Li M, Ji D, Pamudji MS, Lui KH, Zhao Y, Zhao G, Zhou S-Q, Mo C-H, Han W, Yeung KL. Occurrence, risk, and treatment of ciprofloxacin and clarithromycin in drainage. Chem. Eng. J. 2023, 466, 142968. doi:10.1016/j.cej.2023.142968

[2] Mintz I, Chowers M, Obolski U. Prediction of ciprofloxacin resistance in hospitalized patients using machine learning. Commun. Med. 2023, 3, 43. doi:10.1038/s43856-023-00275-z

[3] Shurbaji S, Huong PT, Altahtamouni TM. Review on the visible light photocatalysis for the decomposition of ciprofloxacin, norfloxacin, tetracyclines, and sulfonamides antibiotics in wastewater. Catalysts 2021, 11, 437. doi:10.3390/catal11040437

[4] Kutuzova A, Dontsova T, Kwapinski W. Application of TiO_2-based photocatalysts to antibiotics degradation: cases of sulfamethoxazole, trimethoprim and ciprofloxacin. Catalysts 2021.

[5] Panchangam SC, Yellatur CS, Yang J-S, Loka SS, Lin AYC, Vemula V. Facile fabrication of TiO_2-graphene nanocomposites (TGNCs) for the efficient photocatalytic oxidation of perfluorooctanoic acid (PFOA). J. Environ. Chem. Eng. 2018, 6, 6359–6369.

[6] Wei W, Wang A, Guo K, He S, Li A, Kang X, Fang J. Enhanced degradation of micropollutants by UV/freshly formed colloidal MnO2: reactive species, kinetics and pathways. Appl. Catal. B Environ. 2022, 313, 121441. doi:10.1016/j.apcatb.2022.121441

[7] Li H, Fu B, Huang H, Wu S, Ge J, Zhang J, Li F, Qu P. Catalytic degradation of organic pollutants by manganese oxides: a comprehensive review. Environ. Pollut. Bioavailab. 2022, 34(1), 395–406. doi:10.1080/26395940.2022.2123047

[8] Fan K, Chen Q, Zhao J, Liu Y. Preparation of MnO_2-carbon materials and their applications in photocatalytic water treatment. Nanomaterials 2023, 13, 541. doi:10.3390/nano13030541

[9] Chiam S-L, Pung S-Y, Yeoh F-Y. Recent developments in MnO_2-based photocatalysts for organic dye removal: a review. Environ. Sci. Pollut. Res. 2020. doi:10.1007/s11356-019-07568-8

[10] Oladoye PO, Shokunbi OS, Bamisaye A, Oreofe TA, Olorunfemi KO, Bamigboye MO, Ajiboye OM, Kadhom M, Oladipo SD. Assessing the occurrence and ecotoxicology of ciprofloxacin in aquatic environments: insights into clay-based adsorptive remediation measures. Sci. Total Environ. 2025, 1004, 180738. doi:10.1016/j.scitotenv.2025.180738

(This work is licensed under a Creative Commons Attribution 4.0 International License.)

International Journal of Engineering Research & Technology (IJERT)
ISSN: 2278-0181
Vol. 15 Issue 10 , October - 2026

[11] Malakootian M, Faraji M, Malakootian M, Nozari M. Ciprofloxacin removal from aqueous media by adsorption process: a systematic review and meta-analysis. Desalin. Water Treat. 2021, 229, 252–282. doi:10.5004/dwt.2021.27334

[12] Ehiomogue P, Ahuchaogu II, Ahaneku IE. Review of adsorption isotherms models. Acta Technica Corviniensis – Bulletin of Engineering 2021, 14(4).

[13] Chen H, Gao B, Li H. Removal of sulfamethoxazole and ciprofloxacin from aqueous solutions by graphene oxide. J. Hazard. Mater. 2015, 282, 201–207.

[14] Wang F, Yang B, Wang H, Song Q, Tan F, Cao Y. Removal of ciprofloxacin from aqueous solution by a magnetic chitosan grafted graphene oxide composite. J. Mol. Liq. 2016, 222, 188–194.

[15] Sadek AHS, Xu A, Hassan GK, Zhao L, Zhang Y. Transformation and detoxification of fluoroquinolone antibiotics by singlet oxygen: a review. Sep. Purif. Technol. 2026, 380, 135279. doi:10.1016/j.seppur.2025.135279

[16] Chen P, Zhu Z, Liu Z, Liang F, Zhu X, Bin Z, Huang F, Wang N, Zhu Y. Efficient removal of ciprofloxacin from water by BiOX/GaMOF S-scheme heterojunction: a synergistic effect of adsorption and photocatalysis. Chem. Eng. J. 2025, 506, 159689. doi:10.1016/j.cej.2025.159689

[17] Khan A, Shah AA, Allehabi SO, Ahmed F, Alsulami A, Azam A. Enhanced degradation of ciprofloxacin (CIP) antibiotic and methylene blue (MB) dye using ZnO/GO nanocomposites under solar irradiation. Sci. Rep. 2024, 14, 30696. doi:10.1038/s41598-024-78636-4

[18] Ngo H-S, Nguyen T-L, Tran N-T, Le H-C. Photocatalytic removal of ciprofloxacin in water by novel sandwich-like $CuFe_2O_4$ on rGO/halloysite material: insights into kinetics and intermediate reactive radicals. Water 2023, 15, 1569. doi:10.3390/w15081569

[19] Chahal S, Sahu TK, Kar S, Ranjan H, Ray SJ, Kumar P. Free-standing δ-MnO_2 atomic sheets. Engineering Reports 2023, e12787. doi:10.1002/eng2.12787

[20] Belousov AS, Suleimanov EV, Parkhacheva AA, Fukina DG, Koryagin AV, Koroleva AV, Zhizhin EV, Gorshkov AP. Regulating of MnO_2 photocatalytic activity in degradation of organic dyes by polymorphic engineering. Solid State Sci. 2022, 132, 106997. doi:10.1016/j.solidstatesciences.2022.106997

[21] Khatri M, Gupta A, Gyawali K, Adhikari A, Koirala AR, Parajuli N. Photocatalytic degradation of dyes using synthesized δ-MnO2 nanostructures. Chem. Data Collect. 2022, 39, 100854. doi:10.1016/j.cdc.2022.100854

[22] Worku AK, Ayele DW, Habtu NG. Influence of nickel doping on MnO_2 nanoflowers as electrocatalyst for oxygen reduction reaction. SN Appl. Sci. 2021. doi:10.1007/s42452-021-04746-7

[23] Zhong C, Zhao H, Cao H, Fu J, Xie Y, Sun Z. Acidity induced fast transformation of acetaminophen by different MnO_2: kinetics and pathways. Chem. Eng. J. 2019, 359, 518–529. doi:10.1016/j.cej.2018.11.172

[24] Hu C-Y, Kuan W-H, Lee I-J, Liu Y-J. pH-dependent mechanisms and kinetics of the removal of acetaminophen by manganese dioxide. J. Environ. Chem. Eng. 2021, 9, 105129. doi:10.1016/j.jece.2021.105129

[25] Kekes T, Nika M-C, Tsopelas F, Thomaidis NS, Tzia C. Use of δ-manganese dioxide for the removal of acetaminophen from aquatic environment: kinetic–thermodynamic analysis and transformation products identification. J. Environ. Chem. Eng. 2020, 8, 104565. doi:10.1016/j.jece.2020.104565

[26] Anthony Muliaji. Thesis title "Sunlight/MnO_2 degradation of methotrexate by α-, β- and δ-MnO_2". National Taiwan University, 2024. doi:10.6342/NTU202402891

[27] Alam A, Rahman WU, Rahman ZU, Khan SA, Shah Z, Shaheen K, Suo H, Qureshi MN, Khan SB, Bakhsh EM, Akhtar K. Photocatalytic degradation of the antibiotic ciprofloxacin in the aqueous solution using Mn/Co oxide photocatalyst. J. Mater. Sci.: Mater. Electron. 2022, 33, 4255–4267. doi:10.1007/s10854-021-07619-2

[28] Deng J, Ge Y, Tan C, Wang H, Li Q, Zhou S, Zhang K. Degradation of ciprofloxacin using α-MnO_2 activated peroxymonosulfate process: effect of water constituents, degradation intermediates and toxicity evaluation. Chem. Eng. J. 2017, 330, 1390–1400. doi:10.1016/j.cej.2017.07.137

[29] Khan A, Zhang K, Taraqqi-A-Kamal, Wang X, Chen Y, Zhang Y. Degradation of antibiotics in aqueous media using manganese nanocatalyst-activated peroxymonosulfate. J. Colloid Interface Sci. 2021, 599, 805–818. doi:10.1016/j.jcis.2021.04.095

[30] Zhao J, Wang Y, Li N, Wang S, Yu J, Li X. Efficient degradation of ciprofloxacin by magnetic γ-Fe_2O_3–MnO_2 with oxygen vacancy in visible-light/peroxymonosulfate system. Chemosphere 2021, 276, 130257. doi:10.1016/j.chemosphere.2021.130257

[31] Fu K, Su Y, Yang L, Ji N, Song C, Ma D, Lv X, Han R, Liu Q. Pt loaded manganese oxide nanoarray-based monolithic catalysts for catalytic oxidation of acetone. Chem. Eng. J. (accepted manuscript; PII S1385894721059672).

[32] Reddy MN, Sekhar YC, Sarma LS. Facile electrooxidation of urea on nickel/metal oxide nanocomposites in alkaline media. Mater. Sci. Eng. B 2025, 311, 117785.

[33] Sravani B, Chandrashekar Y, Sri Chandana P, Maiyalagan T, Sarma LS. Bimetallic PtCu-decorated reduced graphene oxide (RGO)-TiO_2 nanocomposite for efficient oxygen reduction reaction. Synth. Met. 2020, 266, 116433.

[34] Yang J-S, Lai WW-P, Panchangam SC, Lin AY-C. Photoelectrochemical degradation of perfluorooctanoic acid (PFOA) with GOP25/FTO anodes: intermediates and reaction pathways. J. Hazard. Mater. 2020, 391, 122247.

[35] Sable SS, Panchangam SC, Lo S-L. Abatement of clofibric acid by Fenton-like process using iron oxide supported sulfonated-ZrO_2: efficient heterogeneous catalysts. J. Water Process Eng. 2018, 26, 92–99.

[36] Muliastri D, Widyartha AB, Wasiara, Saputra R, Nurdin M, Ramadhan LOAN. Nickel slag coated by titanium dioxide for degradation of methylene blue. IOP Conf. Ser.: J. Phys.: Conf. Ser. 2018, 1095, 012009. doi:10.1088/1742-6596/1095/1/012009

[37] Waghchaure RH, Koli PB, Adole VA, Jagdale BS. Exploration of photocatalytic performance of TiO_2, 5% Ni/TiO_2, and 5% Fe/TiO_2 for degradation of eosine blue dye: comparative study. Results Chem. 2022, 4, 100488. doi:10.1016/j.rechem.2022.100488

[38] Tan K-H, Shih Y-H, Chen W-L. Facile preparation of environmental benign LED white light active humic acid nanolayer coated titanium dioxide photocatalyst for bisphenol A degradation. Chemosphere 2024, 355, 141710.

(This work is licensed under a Creative Commons Attribution 4.0 International License.)